ChemElectroChem

Research Article
doi.org/10.1002/celc.202400414

Chemistry Europe
European Chemical Societies Publishing

www.chemelectrochem.org

Surface Nanostructuring of Copper Using Fluoride and Chloride

Vicente Pascual-Llorens,[a] Albert Serra Ramos,[b, c] Pedro Mazaira-Couce,[a, d] María Escudero-Escribano,[a, e, f] and Paula Sebastián-Pascual*[a, g]

Copper is an active electrocatalyst for various energy conversion reactions, but its performance depends on the structure of the active surface sites. In this work, we propose a simple strategy to tailor both the roughness and the active site's geometry of copper. To modify the surface of copper, we oxidize and reduce a copper polycrystalline electrode in 0.1 M solutions containing both sodium fluoride and sodium chloride with different chloride/fluoride molar ratios: (0.1-x) M NaF + x M NaCl. To address the anion effect on the changes in surface geometry, we recorded the voltammetric fingerprints of the modified electrodes using lead underpotential deposition (UPD). The voltammetric analysis suggested that while chloride induces (n10) sites, fluoride promotes an increase in the active surface area and the growth of low-coordinated sites with (110) or (111) geometry. Solutions containing both fluoride and chloride anions induced (n10) motifs covered by nanometric clusters, as observed by scanning electron microscopy, forming a highly defect-rich surface. Our work provides a direct link between electrochemical response and ex-situ structural characterization, and compares, in detail, the effect of chloride and fluoride on the surface nanostructuring of copper.

Introduction

Copper is currently one of the most investigated surfaces due to its unique catalytic properties for different energy conversion reactions.[1–3] Copper has shown promising performance for the electrochemical conversion of different molecules, such as the reduction of carbon dioxide (CO_2) to chemicals and fuels,[2,4,5] or the conversion of biomass-derived molecules to produce valuable chemicals.[6] The efficiency and product distribution of these reactions highly depend on the nature and geometry of the copper active surface sites. For the CO_2 reduction reaction, surfaces with long (100) terrace domains convert the CO_2 to C2 + products such as ethylene whereas (111) sites are more selective toward C1 products like methane.[7–9] The introduction of low-coordinated or (110) step sites in (100) terraces increases the production of C2+ products and selectively form more ethanol.[7,8,10] Recent studies have highlighted that the presence of defect sites[10–12] is critical to efficiently convert the CO_2, with an increase in the production of multicarbon products as the surface roughness increases.[10,12–14] Defect sites are low coordinated sites such as steps and kinks, but also edges and corners on nanoparticulated and rough surfaces. How rough and nanostructured surfaces promote electrocatalytic reactions or which products specifically form is currently under discussion due to the difficulty in experimentally addressing the number and identity of defect sites on copper.[12,15,16] To understand the structure-performance relations on copper, it is necessary to find electrochemical methods to quantitatively address the electroactive surface area (ECSA) and the geometry of the different active surface sites.[15,17] Using methods that correlate an electrochemical response with ex-situ or in-situ structural characterization of the surface will help to establish the synthesis conditions to prepare catalysts with tailored distribution of geometric sites and tuneable catalytic properties.[3,18–20]

Understanding the electrochemical behaviour of well-defined copper single crystalline electrodes is key to determining the structure of more complex surfaces such as nanoparticles, nanostructured, or multifaceted copper.[16,21–24] Traditionally, the electrochemical characterization of catalyst surfaces

[a] V. Pascual-Llorens, P. Mazaira-Couce, M. Escudero-Escribano, P. Sebastián-Pascual
Center for High Entropy Alloy Catalysis, Department of Chemistry, University of Copenhagen, Universitetsparken 5, 2100 Copenhagen, Denmark
E-mail: paulasp@kth.se

[b] A. Serra Ramos
Grup d'Electrodeposició de Capes Primes i Nanoestructures (GE-CPN), Departament de Ciència de Materials i Química Física, Universitat de Barcelona, Martí i Franquès, 1, 08028 Barcelona, Catalonia, Spain

[c] A. Serra Ramos
Institute of Nanoscience and Nanotechnology (IN2UB), Universitat de Barcelona, 08028 Barcelona, Catalonia, Spain

[d] P. Mazaira-Couce
Biobased Chemistry and Technology, Wageningen University & Research, Wageningen, 6708 WG, Netherlands

[e] M. Escudero-Escribano
Catalan Institute of Nanoscience and Nanotechnology (ICN2), CSIC, Barcelona Institute of Science and Technology, UAB Campus, 08193 Bellaterra, Barcelona, Spain

[f] M. Escudero-Escribano
Catalan Institution for Research and Advanced Studies (ICREA), Pg. Lluís Companys 23, 08010 Barcelona, Spain

[g] P. Sebastián-Pascual
Wallenberg Initiative Materials Science for Sustainability, Department of Chemistry, School of Engineering Science in Chemistry, Biochemistry and Health, KTH Royal Institute of Technology, Stockholm, Sweden

Supporting information for this article is available on the WWW under https://doi.org/10.1002/celc.202400414

has been performed by recording the blank cyclic voltammogram (CV) or voltammetric fingerprint of the surface electrode in contact with an electrolyte.[18,25] The blank CVs measure the changes in current density or transferred charge with applied potential. These changes are due to interactions between electrode surface, electrolyte species and solvent. These interfacial processes provide voltammetric features that are characteristic for each crystallographic orientation and, therefore, the blank CVs allow the estimation of the facet-distribution in multifaceted surfaces.[21,26,27] Unlike other surfaces from the platinum-group metals such as Pt or Pd,[28,29] blank CVs on copper surfaces have adsorption/desorption peaks with low intensity in single facets. Consequently, the determination of multiple domains on polycrystalline and nanostructured copper with blank cyclic voltammograms is challenging.[16,30]

Alternatively, the voltammetric lead (Pb) underpotential deposition (UPD) on copper is a valuable tool to address copper surface geometries, as we showed in our previous reports.[16,26] During the lead UPD process, a submonolayer of lead is reversibly adsorbed and desorbed on copper at higher potential values than those of bulk lead deposition. The lead UPD induces intense and sharp features in the voltammetric response whose potential values and shapes are different for each single facet.[31,32] Using this method, we evaluated the facet distribution on copper surfaces that were subjected to different electrochemical treatments. We showed that the electrochemical surface modification of a copper polycrystalline electrode with chloride induces the elimination of (111) sites and the growth of micrometric motifs with *n*(100)x(110) or (n10) sites.[26,33,34] (n10) surfaces are stepped surfaces composed by (100) terraces of *n* length separated by (110) steps. The electrochemical surface modification treatment consisted of applying very fast oxidation/reduction voltammetric cycles in 0.1 M NaCl, to oxidize/dissolve copper at a high anodic potential limit. Then, the dissolved copper is reduced and redeposited on the surface at the applied cathodic potential limit. Further DFT calculations and Wulff constructions supported that chloride acts as a ligand agent that strongly adsorbs on (n10) domains, stabilizing their surface energies and favouring their growth over other facets.[26,35] By simply modulating the electrochemical parameters during the oxidation/reduction of copper with chloride, such us anodic oxidation limit, number of cycles or scan rate, we could tune the (n10)/(111) sites ratio on copper.

Although chloride induces surface refaceting on copper, it does not significantly change its electroactive surface area and instead forms large micrometric (n10) motifs nearly 1 μm in size. Increasing the electroactive surface area relative to the geometric area of the electrode, as well as changing the surface structure, are crucial parameters to achieve high conversion rates. In this work, we present a new strategy to induce surface nanostructuring and increase the electroactive surface area of copper electrodes with (n10) or (100)x(110) motifs. Our method consists of carrying out the electrochemical surface modification treatment of copper with 0.1 M solutions containing both fluoride and chloride anions: (0.1-x) M NaCl + x M NaF. Previous reports investigated the effect of different halides such as chloride, bromide or iodide, on the change in surface structure of copper[34,36] or other model catalysts, such as palladium.[37] These works showed that the nature of the anion induces different surface morphologies, allowing the tuning of the active site's geometry and the catalytic properties of the electrode surface. Unlike chloride or the larger halides, fluoride adsorption on metallic surfaces and in aqueous electrolytes is typically weak.[38,39] Density functional theory (DFT) calculations performed by I.T. McCrum et al.[40] illustrated that fluoride adsorption on Cu(100), Cu(111) and Cu(211) surfaces is less favourable compared to other halides, a fact that was ascribed to the largest solvation energy of fluoride in aqueous solution. Based on these findings, we have hypothesized that fluoride will primarily induce surface roughness or disorder on copper due to the weak adsorption of fluoride on copper. We started carrying out a comparative study in which we have addressed, in separated experiments, the effect of both chloride and fluoride anions on the surface reconstruction of copper. To do that, we performed the surface modification of copper in either 0.1 M NaCl or 0.1 M NaF solutions. Later, we evaluated the combined effect of fluoride and chloride on the surface modification of copper by using (0.1-x) M NaCl + x M NaF solutions, and we varied the (0.1-x) NaCl/ x NaF molar ratio to tune the active sites distribution and the surface roughness on copper. To address the change in surface structure and electroactive surface area, we recorded the lead UPD CVs on the prepared surfaces. Then, we compared the voltammetric response of the modified surfaces with the lead UPD CVs of several model single facets to address the geometry of the surface sites of the modified copper electrodes. Our work has a double purpose: 1) to establish new strategies to rationally tune the surface structure and increase the electroactive area of copper by using electrodeposition methods, 2) find a direct link that correlates with an electrochemical response or voltammetric fingerprint of copper with nanoscale structural characterization of the surface morphology, which is key to prepare well-defined nanostructured catalysts.

Experimental Methods

Electrochemical Methods

All electrochemical experiments were carried out in a classical three-electrode glass cell with four entries and a luggin capillary for the reference electrode. The reference electrode was a saturated calomel electrode (SCE). This reference electrode has been previously used in the original works by Brisard and co-workers[31,32] in which the lead UPD on Cu single facets was addressed in perchlorate solutions. Stable and reproducible values of the potential were obtained for the UPD deposition of lead on copper. For these reasons and to better compare our results with the previous reports on the lead UPD on copper and in perchlorate solutions, we have referred the potentials of the voltammetric analysis of this work to the SCE reference electrode. Figure S1 contains the CVs of several copper facets vs SCE (Figure S1A) and vs the reference hydrogen electrode (RHE) (Figure S1B) as the RHE is commonly used in electrocatalysis. We have calibrated the SCE by measuring the potential difference between the SCE and a reversible hydrogen electrode (RHE) at different pH values. To

prepare the RHE electrode, we immersed a platinum wire in different solutions containing 1.0 M (pH 0), 0.1 M (pH 1) and 0.01 M (pH 3) of hydrochloric acid (HCl 37%, Fisher Chemical) and saturated by hydrogen (H_2). The theoretical potential difference between the SCE and the RHE is: E_{SCE}-$E_{RHE} = 0.244 + 0.059 \cdot pH$, where the $E_{SCE} = 0.244$ V[41] whereas the $E_{RHE} = E_{SHE} - 0.59 \cdot pH = -0.59 \cdot pH$. As a counter electrode we used a Cu wire. The working electrodes used in this work were: a Cu polycrystalline electrode (Cu(poly)), and several single facets: Cu(111), Cu(100), Cu(110) and Cu(310) with 99.999% purity and purchased from Mateck company. The electrodes were disks with 5 to 6 mm diameter and had a thickness of 5 mm or more. All experiments have been performed with the working electrode in the hanging meniscus configuration under argon atmosphere to ensure that only the analysed single facet or Cu(poly) surface was in contact with the electrolyte.

Prior to the electrochemical experiments, the Cu(poly) surface was manually polished to mirror-like surface using a suspension of alpha alumina particles (Struers) with diameter of 1 μm, 0.3 μm and 0.05 μm, respectively. Afterwards, it was sonicated five times for 60 seconds in ultrapure water (18.2 MΩ·cm, Milli-Q®). The counter electrode was cleaned by submerging it in a 1:1 volumetric solution of ultrapure water and nitric acid (70%, Fisher Chemical), followed by rinsing it with ultrapure water.[42,43] Afterwards, the working electrode was electropolished in a two-electrode cell containing a 70% phosphoric acid solution (prepared from H_3PO_4, 85%, VMR Chemicals, Prolabo®). Then, we applied a constant potential difference (ΔE) of 2.0 V between the Cu(poly) (anode) and a copper wire (cathode) for 30 seconds. We also pretreated the Cu single facets by electropolishing them in the phosphoric acid solution and by applying a potential difference of 1.8 V between the Cu single facet and the counter electrode. Finally, the electropolished surfaces were rinsed with ultrapure water to remove the excess of acid and were transferred to the electrochemical cell. All the electrochemical experiments have been done using a VSP-300 biologic multipotentiostat (BioLogic).

Before running the experiments, the glassware and the glass cells were kept in a saturated solution of $KMnO_4$ (Sigma Aldrich, Emplura®) overnight to oxidize all organic pollutants. Afterwards, the glassware was rinsed with a diluted solution of H_2O_2 (33%, VMR Chemicals, Prolabo®) + H_2SO_4 (96%, Sigma Aldrich, Suprapur®), to remove the MnO_2 waste, and was boiled three times in ultrapure water.

Surface Modification of Copper by NaCl and NaF

At first, we performed the electrochemical roughening of copper in either 0.1 M NaCl or 0.1 M NaF solutions aiming to assess, separately, the effect of these two different anions on the copper surface reconstruction. After that, we carried out the electrochemical roughening treatment in solutions containing (0.1-x) M NaCl + x M NaF with different Cl^-:F^-:molar ratios to address the combined effect of chloride and fluoride on the copper surface reconstruction. Additionally, we have also performed the electrochemical roughening of the Cu(poly) in 0.02 M NaCl + 0.08 M $KClO_4$ solutions. To induce the surface modification of copper with Cl^- and F^- halides, we applied and oxidation/reduction treatment that consisted in cycling the copper electrode from −1.0 V vs SCE to different anodic or oxidation potentials (1.0 V and 2.0 V vs SCE) and to −1.0 V for the redeposition of copper. The cyclic voltammetry of the oxidation/redeposition of copper in 0.1 M halide solution was carried out at a high scan rate of 200 $mV \cdot cm^{-2}$ (Figure S2) to tailor the degree of surface reconstruction on copper by changing the anodic potential limit.[26] After performing this oxidation/reduction treatment, the electrode was consecutively cycled at 500 $mV \cdot s^{-1}$ in the same solution but in the double layer potential region between −1.0 V and −0.40 V vs SCE to remove the traces of copper chloride, copper fluoride or copper oxide on the surface as we reported in our previous publication.[26] This cleaning step was necessary to perform the lead UPD on a metallic copper surface, as the lead UPD does not display features, or the features are broad and highly irreversible if the surface remains covered by a cooper oxide or copper halide layer.

Determination of the Electroactive Surface Area and Facet Distribution by Lead Underpotential Deposition (UPD)

The cyclic voltammograms (CVs) of the lead (Pb) underpotential deposition (UPD) on the reconstructed Cu(poly) and the electropolished Cu(poly), as well as on the different copper single facets were performed in an electrolyte solution containing: 0.1 M $KClO_4$ (99.95%, Sigma-Aldrich Merck) + 2 mM of NaCl (99.9% Sigma-Aldrich Merck) + 2 mM of $Pb(ClO_4)_2 \cdot H_2O$ (99.995%, Sigma-Aldrich Merck) + 1 mM $HClO_4$ (70%, Sigma Aldrich Merck, Suprapur®), and the pH of the solution was kept at 3. We added chloride to the solution containing lead because chloride enhances the lead UPD kinetics. Chloride induces sharp voltammetric peaks in the CV of each single facet, allowing to decouple the different facet contributions on the polyoriented and on the reconstructed copper surfaces.[31,32] All the lead UPD cyclic voltammograms of this work were performed between −0.4 V and −0.2 V vs SCE with a slow scan rate of 5 $mV \cdot s^{-1}$ as metal UPD is a process with slow kinetics.[44] In addition to that, we have also recorded the blank CVs of the Cu single facets in contact with 0.1 M $KClO_4$ + 2 mM NaCl + 1 mM $HClO_4$, i.e., in the absence of lead (Figure S1A and B, insets). These blank CVs were recorded at 5 $mV s^{-1}$ in the potential region between −0.15 V and −0.45 V vs SCE. Moreover, we have also registered the electrochemical windows of the Cu single facets, in the same electrolyte and with no Pb in solution to corroborate that the lead UPD features do not overlap with the oxidation of the copper surface (Figure S1C). The electrochemical windows were recorded at 50 $mV \cdot s^{-1}$.

We calculated the ECSA of the different copper electrodes by integrating the charge involved in the cathodic curve of the lead UPD CVs.[16,45] The roughness factor (RF) determines the variation of the ECSA on each halide-modified copper surface. The RF was determined by calculating the ratio between the integrated charge of each halide-modified copper and the integrated charge of the extended Cu(poly) flat surface, with roughness factor nearly equal to 1.[26] To determine the RF we have used the following equation:

$$RF = \frac{Q_{Cu(reconstructed)}}{Q_{Cu(poly)}} \quad (1)$$

Where $Q_{Cu(reconstructed)}$ is the integrated charge in the cathodic curve of lead UPD on each reconstructed Cu surface ($\mu C \cdot cm^{-2}$) and $Q_{Cu(poly)}$ is the integrated charge in the cathodic curve of lead UPD of Cu(poly) flat surface ($\mu C \cdot cm^{-2}$).

On the other hand, we have recorded the lead UPD CVs on the different single facets to determine the preferential facet or the geometry of the sites in the reconstructed copper surfaces using the NaF and NaCl solutions. We used the peak-potential values in the lead UPD CVs of the Cu single facets as a reference to identify the different single facet-peak contributions in the halide-modified copper surfaces.

Morphology Analysis

Before the ex-situ morphological characterization using Scanning Electron Microscopy (SEM), the modified samples were cleaned by cycling the electrode at 500 $mV \cdot s^{-1}$ and in between −0.4 V and −0.2 V vs SCE in the sodium halide solution used for the electrochemical roughening of copper. The SEM analysis was performed before and after the lead UPD to confirm that the lead adsorption/desorption on copper does not significantly modify the copper surface morphology. Then, the samples were cleaned with abundant ultrapure water. The morphology of the halide-treated samples was analysed using both a JEOL 7800 F prime scanning electron microscopy (SEM) from the University of Copenhagen, at low voltage (4 KeV), and a field emission scanning electron microscope (FE-SEM; JSM-7100 F Analytical Microscopy) from CCiTUB, to gain more resolution at the nanometric scale.

X-Ray Photoelectron Spectroscopy (XPS) Analysis

XPS experiments were conducted at CCiTUB using ESFOSCAN, which is based on the PHI 5000 VersaProbe instrument from Physical Electronics (ULVAC-PHI). The measurements were performed with a monochromatic focused X-ray source (Aluminium Kalfa line of 1486.6 eV) that was calibrated using the $3d_{5/2}$ line of Ag with a full width at half maximum of 0.6 eV. The analyzed area was a circle with a diameter of 100 microns. The spectra were taken with a resolution of 224 eV of Pass Energy and 0.8 eV/step for the general spectra and 27 eV of Pass Energy and 0.1 eV/step for the high-resolution spectra of the selected elements. To discharge the powders, when necessary, a combination of a low-energy electron gun (less than 10 eV) and a low-energy ion gun (Ar ions at less than 5 eV) was used. The measurements were conducted in an ultra-high vacuum (UHV) chamber with a pressure ranging from 5×10^{-10} to 5×10^{-9} Torr.

Results

We started recording the voltammetric lead UPD curves on different Cu single facets and in the 0.1 M $KClO_4$ + 1 mM $HClO_4$ + 2 mM $Pb(ClO_4)_2$ + 2 mM NaCl solution, which appear in Figure S1: Cu(111), Cu(100) and Cu(110) as well as the Cu(310) which is a 3(100)x(110) stepped surface. The CVs in Figure S1 are essentially the same as those in our previous work and have a different profile for each crystallographic orientation.[26] All the CVs profiles present intense peaks in the cathodic region, where lead is underpotentially deposited, whereas the peaks in the anodic region, where lead is desorbed, are broader and non-symmetric. Figure S1 also shows the blank CVs of the copper basal planes in contact with the same electrolyte (0.1 M $KClO_4$ + 2 mM NaCl + 1 mM $HClO_4$) and in the absence of lead in the solution. The recorded currents of the blank CVs are several magnitudes lower than the intense current peaks of the lead UPD CVs on Cu, in good agreement with the previous works by Brisard and co-workers.[31] The asymmetry and irreversibility of the lead UPD peaks in Figure S1 could be due to the formation of a subsurface Pb–Cu alloy,[21] or because the lead UPD kinetics are kinetically slow.[31,32] In this report, we have used the CVs of the copper single facets as a reference to address which preferential surface orientations and sites are induced after electrochemically modifying copper with chloride and fluoride. To address the change in surface structure, we have primarily analysed the cathodic region of the lead UPD curves, where the single-facet peaks are more separated, being easier to decouple in the CV..

After recording the lead UPD CVs on the copper single facets, we have evaluated, the effect of fluoride anions on the surface modification of copper and we have compared it with the chloride effect on the copper reconstruction. To perform the surface modification on copper we have applied an oxidation/reduction treatment following a similar procedure that the one in our previous studies and explained in the Experimental Methods section.[16,26] We control the degree of surface reconstruction or facet modification by applying different oxidation potential limits (E_{ox}) in the solution of 0.1 M sodium halide. Figure 1 contains the lead UPD voltammetric response of a modified Cu(poly) electrode using either 0.1 M NaCl (Figure 1A) or 0.1 M NaF (Figure 1B) and at two different oxidation potentials (E_{ox}): 1.00 V and 2.00 V vs SCE. Both panels A and B present the lead UPD profile of the non-modified Cu(poly) (black line) to illustrate the anion effect on the copper surface reconstruction. Figure 1A shows that the modification of the Cu(poly) with 0.1 M NaCl causes that the peak at −0.32 V vs SCE, which corresponds to the (111) facet (Figure S1) decreases in intensity. In addition, a peak at −0.35 V vs SCE arises when we increase the applied oxidation potential during the oxidation/reduction surface modification treatment in 0.1 M NaCl. This peak is close to the (310) facet peak (Figure S1), showing that chloride preferentially induces the growth of (n10) sites, as we reported in our previous report.[26] Figure 1B shows the lead UPD response of the Cu(poly) modified by fluoride. Unlike chloride, the fluoride anion only causes a broadening of the main features of the Cu(poly) in the lead UPD CV, suggesting that fluoride primarily induces surface roughness and disordering. The increase in the ECSA and RF of copper is more pronounced when we modified it with the 0.1 M NaF solution, especially at high applied anodic potentials (E_{ox} = 2.0 V). Table 1 summarizes the RF of the copper surfaces restructured in each halide solution. The fluoride anions induce a RF of 1.82 ± 0.06 when the E_{ox} is 2.0 V, whereas the chloride anion produces a minor increase of the RF which is 1.29 ± 0.05

Table 1. Integrated charge values of the cathodic region and roughness factors (RF) of lead UPD CVs on Cu surfaces treated with chloride and/or fluoride.

$[Cl^-]$ = 0.1 M			
Upper Limit/V	Cycles	Charge/$\mu C \cdot cm^{-2}$	RF
1	3	390 ± 7	1.12 ± 0.02
2	3	448 ± 20	1.29 ± 0.05
2	10	598 ± 23	1.58 ± 0.06
$[F^-]$ = 0.1 M			
Upper Limit/V	Cycles	Charge/$\mu C \cdot cm^{-2}$	RF
1	3	422 ± 49	1.21 ± 0.15
2	3	637 ± 16	1.82 ± 0.06
2	10	2114 ± 174	5.98 ± 0.44

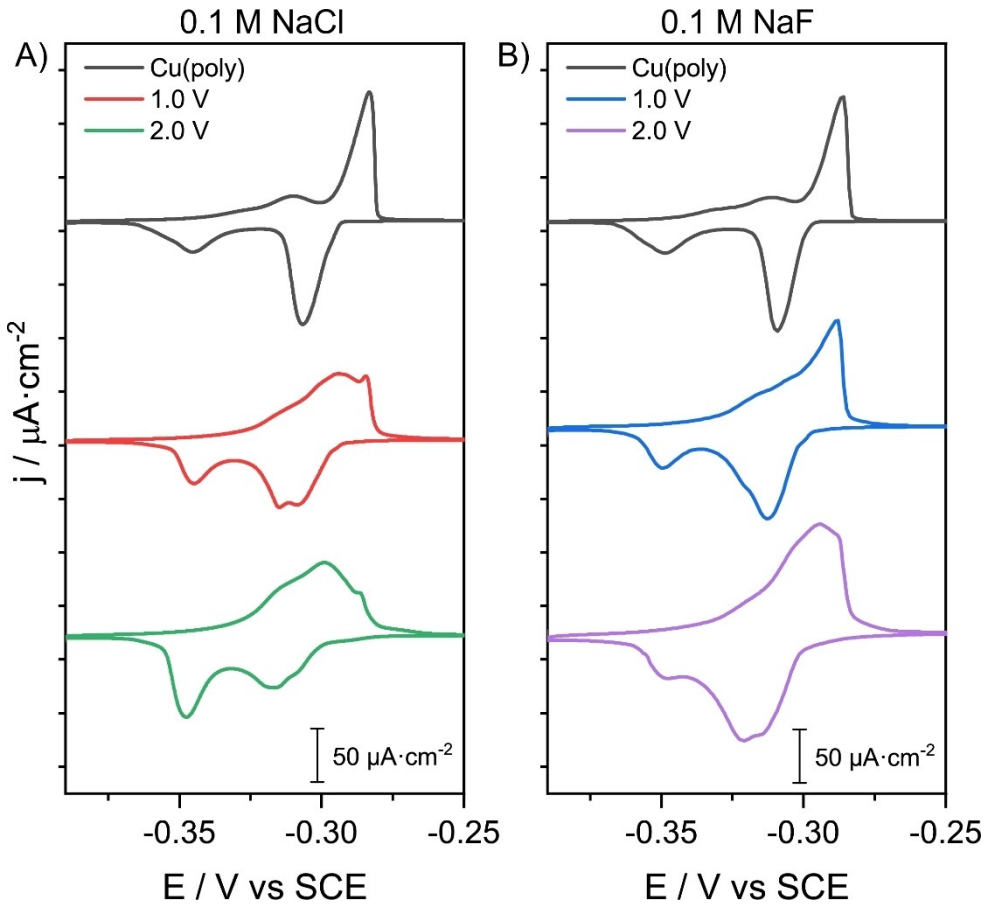

Figure 1. Lead UPD CVs on modified Cu(poly), recorded in a 0.1 M $KClO_4$ + 2 mM NaCl + 1 mM $Pb(ClO_4)_2$ solution. The Cu(poly) surfaces have been modified using two different solutions containing A) 0.1 M NaCl and B) 0.1 M NaF by applying three consecutive voltammetric cycles with oxidation potential limits of 1.0 V and 2.0 V vs SCE.

at E_{ox} of 2.0 V. We note that the lead UPD CVs remain stable upon three to five consecutive cycles for each modified surface, as we reported in our previous work.[26]

After evaluating the effect of chloride and fluoride in the surface modification of copper, we have addressed the morphology of the reconstructed samples ex-situ and by using SEM. Figure 2A shows the morphology of the Cu(poly) reconstructed in 0.1 M NaCl after applying an oxidation potential of 2.0 V vs SCE. The SEM showed the formation of large areas with highly stepped motifs nearly 1 μm of size, and with the shape of tetragonal pyramids. This morphology aligns with the lead UPD voltammetric response that suggests that chloride induces the preferential formation of (n10) domains.[26,46] Figure 2B shows the chloride-induced modification in a new Cu(poly) sample, with a higher magnification, to illustrate the formation of pyramids with defined shape, in which the four sides may contain (n10) sites and the base likely has (100) sites.[26,46] Figure 2C shows the results on the Cu(poly) modified in 0.1 M NaF solution. The SEM does not show any specific shape or feature. Instead, it shows a surface with tiny holes. Figure 2D shows a magnification of the copper surface treated with fluoride, where we can appreciate several wholes of nanometric size. This result supports that fluoride essentially induces surface roughness or disorder, in line with the CV in Figure 1B. In Figure S3, we displayed the SEM image of a polished Cu(poly), before being electrochemically modified by the halides, which is relatively flat and displays different grain domains.

To better address the effect of fluoride on the increase in active area of copper, we applied a more aggressive oxidation/reduction surface modification treatment in which we increased the number of voltammetric cycles to 10. Figure 3 shows the lead UPD CVs of a Cu(poly) treated in 0.1 M NaCl solution (Figure 3A) and in 0.1 M NaF solution (Figure 3D), and by applying 3 (black line) and 10 (red line) oxidation/reduction cycles between −1.0 and 2.0 V vs SCE. The lead UPD profile of the 10-cycles sample modified with 0.1 M NaCl (Figure 3A) displays a slightly higher cathodic charge than the 3-cycles sample, with a RF of 1.54 and a lower ratio of (n10)/(111) domains. The SEM image in Figure 3B shows large areas with a random distribution of pyramids. Figure 3C shows a magnification of these areas which are also stepped, but slightly less defined than in Figure 2B. It is important to note that the surface modification treatment, which is essentially an electrodeposition process of copper onto copper, is highly sensitive to the quality and structure of the substrate. Some electrode areas, surface imperfections, grain boundaries seem to activate the electrochemical surface modification process and cause corro-

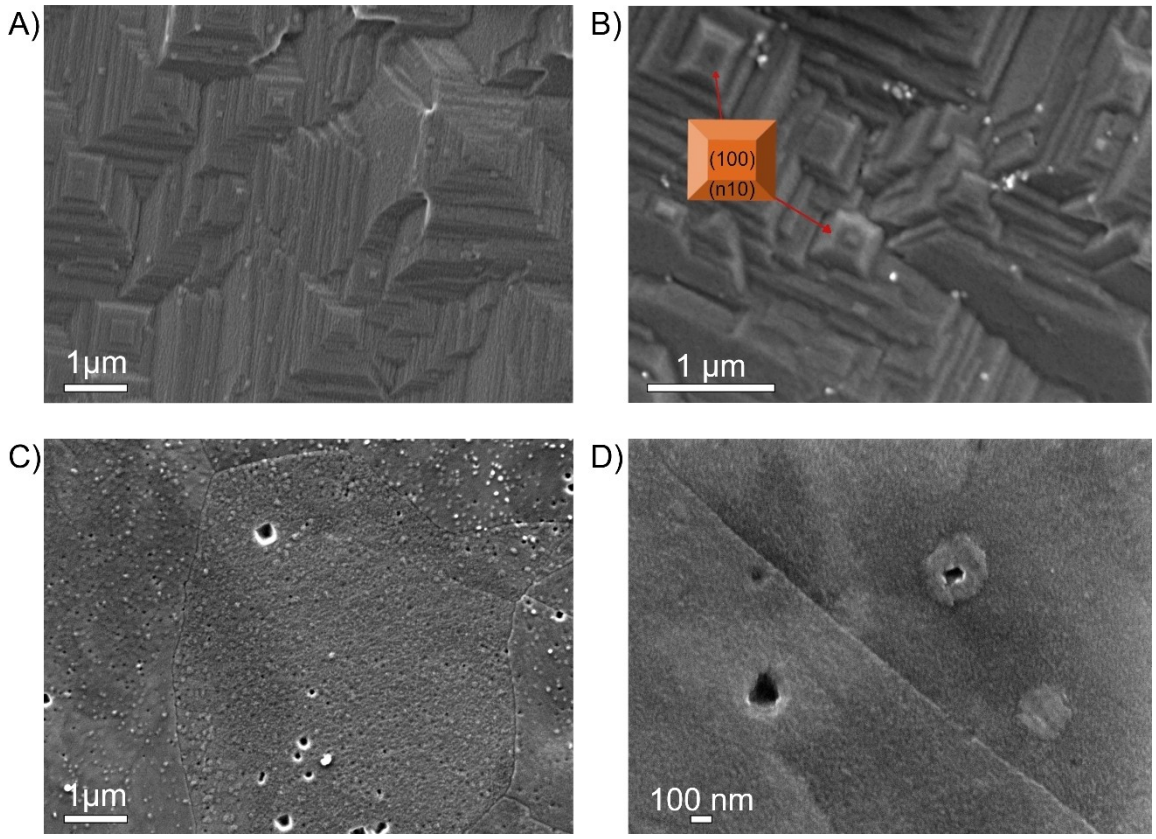

Figure 2. SEM images of: A) and B) Cu(poly) surfaces restructured in 0.1 M NaCl solution after applying three consecutive potential cycles between −1.0 V and 2.0 V vs SCE; C) and D) Cu(poly) surface restructured in 0.1 M NaF solution after applying three consecutive potential cycles between −1.0 V and 2.0 V vs SCE.

sion with signs of pitting on the electrode, as shown in Figure S4. Despite that, there is a tendency of forming a morphology that it is stepped as also illustrated in Figure S4 which supports that chloride favours the growth of (310) or (n10) facets. Figure 3D shows the CV of the Cu(poly) modified by NaF after applying 3 and 10 oxidation/reduction cycles. The treatment with ten cycles in NaF induces a notable increase of the ECSA of the copper surface. The 10-cycles sample has a RF of 5.98, which is about 3 times higher than the RF of the 3-cycles sample, as shown in Table 1. The SEMs images of the 10-cycles sample in Figure 3E displays the formation of micrometric wholes with a high population of dendrites (Figure 3F), which could explain the significant increase in active surface area. To test this hypothesis, we have sonicated the samples in water to remove the dendrites, which are lowly adherent. Figure S5 shows the lead UPD CVs of the 10-cycles sample treated in the NaF solution before and after sonicating them in ultra-pure milli-q water for 60 seconds. Sonicating the 10-cycles electrode with water considerable reduces the ECSA of the electrode from 6 to 2.6, showing that fluoride can form surfaces with high active area, but they are not stable.

After addressing the effect of chloride and fluoride on the restructuration of copper, we modified our Cu(poly) with solutions containing both fluoride and chloride but with different Cl^-:F^- molar ratios, to tune both the active surface area and the formation of (n10) sites. We used the same oxidation/reduction electrochemical treatment than in Figure 1. We modified our Cu(poly) electrode using 0.1 M solutions with variable (0.1-x) Cl^-:x F^- molar ratios of: 0.08 Cl^-:0.02 F^-, 0.05 Cl^-:0.05 F^-, 0.04 Cl^-:0.06 F^- and 0.02 Cl^-:0.08 F^-. To better explain the combined effect of fluoride and chloride on the surface modification of copper, we plotted in Figure 4A the lead UPD CVs after applying the modification in separated 0.1 M NaCl and in 0.1 M NaF solutions, whereas Figure 4B shows the lead UPD CVs after performing the surface modification in the (0.1-x) M NaCl + x M NaF solutions. Figure 4A clearly shows that fluoride (red curves) induces an increase of the charge in the voltammetric region between −0.30 V and −0.35 V which corresponds to the region of the (110) and (111) single facets (Figure S1). However, the feature cantered at −0.35 V, corresponding to the (n10) facet, is less intense with fluoride, whereas with chloride the (n10) peak is the most intense feature. The lead UPD curves in Figure 4B shows that modifying copper with mixtures of fluoride and chloride, generates surfaces with both (n10) domains and high active area or RF. The pink curve shows the lead UPD of a Cu(poly) modified in a 0.08 Cl^-:0.02 F^- molar ratio solution which is similar to the lead UPD CV obtained in 0.1 M NaCl although with a less prominent (n10) peak. A progressive increase of the content of fluoride in solution, from 0.5 Cl^-:0.5 F^- (blue curve) to 0.04 Cl^-:0.06 F^- (green curve) and to 0.02 Cl^-:0.08 F^- (grey curve) molar ratios, causes an increase of the cathodic charge in the potential

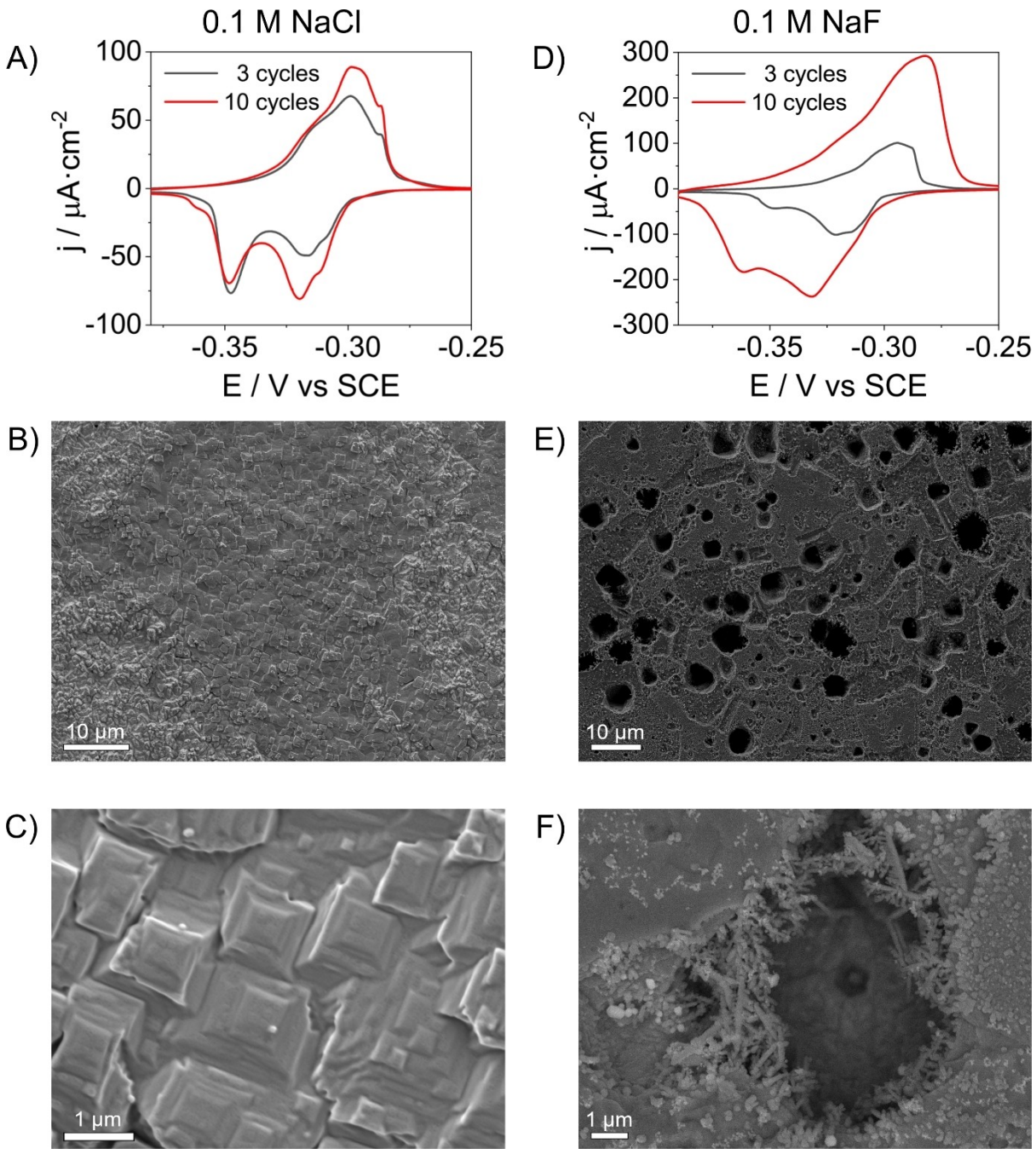

Figure 3. Lead UPD CVs and SEM images of Cu(poly) surfaces which have been reconstructed using: A), B) and C) a 0.1 M NaCl solution; D), E) and F) 0.1 M NaF solution. Figures A) and D) shows the lead UPD CVs of Cu(poly) surfaces which have been modified after applying three (black lines) and ten (red lines) consecutive voltammetric cycles.

region between −0.30 V and −0.35 V. The determination of the ECSA values is summarized in Table 2. Lower fluoride concentrations do not significantly change the ECSA, leading to a RF value of 1.20 for 0.08 Cl^-:0.02 F^- solutions. Higher fluoride concentrations increase the ECSA, achieving the highest RF of 2.80 for the 0.02 Cl^-:0.08 F^- solution. Interestingly, the (n10) peak cantered at −0.35 V vs SCE does not disappear if there are chloride anions in the bath solution used to reconstruct the Cu(poly). In summary, the lead UPD CVs in Figure 4B have features that are a combination of the features in Figure 4A,

Table 2. Integrated charge values of the cathodic region and roughness factor (R.F.) of the lead UPD CVs on Cu(poly) surfaces modified or reconstructed using different (0.1-x) M NaCl + x M NaF solutions.

$[Cl^-]+[F^-]=0.1$ M		
$[Cl^-]:[F^-]$/M	Charge/µC·cm^{-2}	R. F.
0.08:0.02	427 ± 35	1.20 ± 0.09
0.05:0.05	544 ± 8	1.55 ± 0.01
0.04:0.06	820 ± 1	2.31 ± 0.05
0.02:0.08	991 ± 53	2.80 ± 0.15

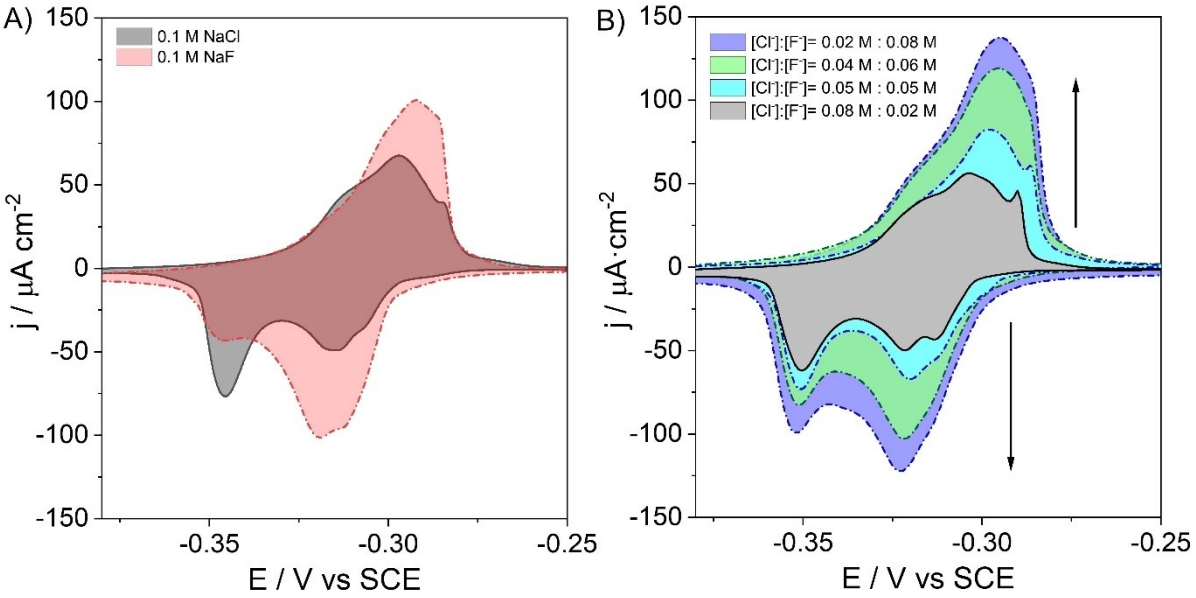

Figure 4. Lead UPD CVs of Cu(poly) surfaces modified in separated solutions of: A) 0.1 M NaCl (black solid line) and 0.1 M NaF (red dashed line) solutions; B) different (0.1-x) M NaCl + x M NaF solutions. Three consecutives voltammetric cycles with applied potential between −1.0 V and 2.0 V vs SCE were run in the different 0.1 M sodium halide bath solutions.

showing the combined effects of both chloride and fluoride on the surface modification of copper.

After modifying copper using chloride and fluoride mixture-solutions, we addressed the change in morphology with SEM. Figure 5A shows the SEM image of a Cu(poly) modified in a solution with 0.06 $^{Cl-}$: 0.04 F^- molar ratio which essentially exhibits the characteristic pattern with tetragonal pyramids induced but chloride. If the concentration of fluoride is nearly equal to the concentration of chloride, the modified surface begins to show signs of disorder as seen in Figure S6A, as well as the formation of nanometric islands or clusters, as illustrated in Figure 5B. Figure 5C displays the SEM image of a copper surface modified using a solution containing 0.04 M Cl^- and 0.06 M F^-. The surface exhibits micrometric tetragonal structures covered by a dense population of nanometric clusters. These SEM observations align well with the electrochemical responses in Figure 4B. In Figure 4B, the lead UPD CVs show that the (n10) peak at approximately −0.35 V vs SCE is consistently present across all curves. Notably, the features between −0.30 V and −0.33 V vs SCE become more pronounced when the fluoride concentration exceeds that of chloride in the solution. This increase in current density in the voltammetric region corresponding to (111) or (110) facets correlate with the formation of nanometric clusters observed in Figures 5B and 5C. Further increasing the fluoride concentration to 0.08 M while maintaining chloride at 0.02 M (Figure S6B and C) results in the coalescence of these nanoclusters. However, the micrometric patterns induced by chloride remain visible in various regions of the electrode surface.

XPS analysis was used to examine the chemical state of the copper surface after the surface modification treatment in NaCl and NaF solutions. We have carried out the XPS right after the electrochemical roughening treatment, and after electrochemically cleaning the samples and removing the halide and oxide layer derived from the oxidation/reduction treatment (Figure 6). The survey spectra showed strong Cu signals and weak O and Cl signals, while the F signal was negligible. For all samples, the sputtering time for the depth profile was 900 seconds in intervals of 30 seconds. The first two spectra for Cu and O presented some singularities, while the rest of the spectra remained constant as the depth of the analysis increased. In the case of Cu 2p, two intense and sharp peaks at 932.6 eV and 952.8 eV, that correspond to Cu $2p_{3/2}$ and Cu $2p_{1/2}$, respectively, were observed in all spectra.[47,48] These peaks were ascribed to Cu_2O or to Cu(0) when the O 2s peaks disappeared after consecutive sputtering cycles (Figure S7), as both Cu_2O and Cu(0) XPS features overlap in the spectra.[49,50] The spectra of Cu treated with NaCl and Cu treated with NaF were identical. However, in the case of Cu treated with NaCl, two faint peaks at 934.8 eV and 954.2 eV corresponding to Cu(II) were observed, although they were less intense. These singularities were only slightly observed in the first cycle and disappeared as the chemical nature was analyzed in depth. For O 2s, the first two layers showed an asymmetric peak with three contributions, especially in the case of Cu treated with NaCl. This peak can be deconvoluted into three peaks with binding energies at approximately 530.8, 531.7, and 532.8 eV, which are assignable to M–O, M–OH, and adsorbed water. When samples were treated with NaF, the signal became practically negligible after a few sputtering cycles, confirming the metallic nature of Cu. However, it should be noted that the intensity of these signals was significantly lower than that of the Cu 2p signals. For the samples treated with NaCl, a small amount of chlorine was detected in both the first and subsequent layers, as evidenced by the Cl 2p peaks. Conversely, in the case of the samples treated with NaF, the amount of fluorine was negligible, as only

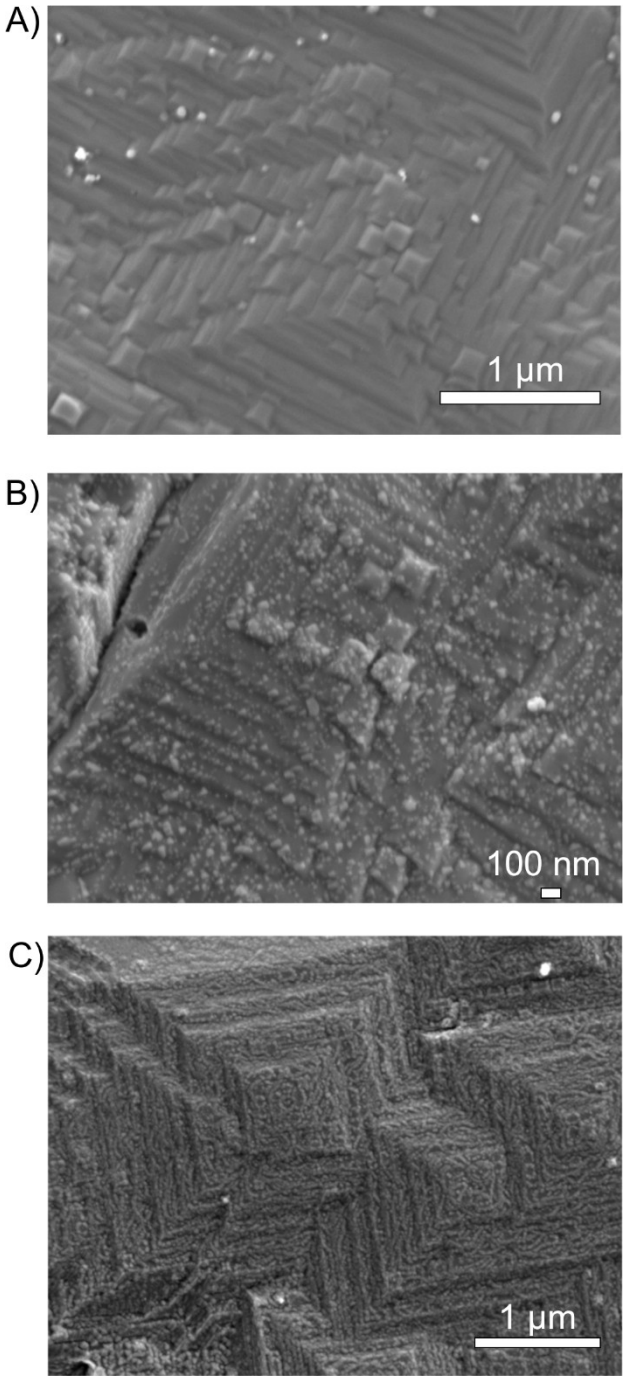

Figure 5. SEM image of a Cu(poly) surfaces which have been modified in: A) 0.06 M NaCl and 0.04 M NaF solution; B) 0.05 M NaCl and 0.05 M NaF solution, and C) in 0.04 M NaCl and 0.06 M NaF solution. To carry out the surface modification, we have applied three consecutive voltammetric cycles between −1.0 V and 2.0 V vs SCE in each bath solution.

a small amount was detected. These results suggest that chloride is strongly adsorbed on copper inducing surface refaceting. In contrast, the XPS analysis shows that fluoride weakly interacts with copper and is mainly dissolved in water. This fact suggests that we could be generating a copper oxide surface during the electro-roughening treatment in 0.1 M NaF that leads to the formation of a rough metallic surface when the copper oxides layer is electrochemically reduced (Figure S2 shows the reduction of oxide-derived copper in 0.1 M NaF).

When the samples were electrochemically cleaned to remove the copper halide or oxide layer, the concentrations of chloride or fluoride were negligible as shown in the XPS analysis (Figure 6, electrochemical cleaning panel). The O 1s peak in both samples disappeared after a few sputtering cycles, supporting that the inner layers of the electrochemically induced motifs are metallic copper. Since the XPS analysis was carried out ex-situ (i.e., the copper samples were exposed to air before being analyzed with XPS), the formation of a surface oxide layer, such as Cu_2O, was inevitable. To confirm that the electrochemical lead UPD is occurring on metallic copper, we carried out the lead UPD on Cu(poly) (Figure S8A) and on Cu(111) (Figures S8B) before and after electropolishing the surface. It is worth noting that cyclic voltammetry is a surface-sensitive technique and has been widely employed to test the surface cleanliness and quality of different metals.[22,23,25] When the Cu(poly) surface was not electrochemically pretreated, the lead UPD CV displayed broad and highly irreversible features. The lead UPD CV of Cu(111) was almost suppressed demonstrating that electrochemical surface cleaning is a critical step in removing the surface oxide layer and contaminants on copper surfaces.

Despite the adsorption of fluoride on copper is weak, its presence in solution significantly increases the active surface area and induces surface roughness and nanostructuring. To confirm that this increase in surface area is not merely due to a decrease in chloride concentration in the (0.1-x) M NaCl + x M NaF solution, we conducted surface modifications treatments using two different fluoride-free solutions: Figure S7A shows the lead UPD of a Cu(poly) modified in a 0.02 M NaCl solution. Figure S7B shows the lead UPD CV of the Cu(poly) modified in a solution containing 0.02 M NaCl + 0.08 M $KClO_4$, as perchlorate anions do not specifically adsorb on metallic surfaces either.[39,51] Both lead UPD curves are overlapped with the lead UPD of a Cu(poly) modified in the 0.02 M NaCl + 0.02 M NaF solution. Figures S9A and S9B confirms that the increase in electroactive surface area is related with the presence of fluoride in the bath solution. The grey curve in Figure S9A (0.02 M NaCl) has a RF of 1.13 and a prominent peak a −0.35 V vs SCE, showing that in the absence of fluoride, the chloride effect dominates on the surface modification of copper. Figure S9B shows that the lead UPD of the Cu(poly) modified in the 0.02 Cl^-:0.08ClO_4^- solution has an area only slightly higher than the Cu(poly) modified in the 0.02 M NaCl solution with a RF of 1.53. Previous studies with platinum electrodes showed that, although neither fluoride nor perchlorate adsorbs specifically on the metallic surface,[38,52] fluoride can affect the kinetics of the adsorption of OH^- groups on e.g. Pt(111)[39] due to a change in the electric double layer structure. Based on these platinum findings, we hypothesize that the increase in active surface area with fluoride may relate to changes in the electric double layer structure, which affects the copper oxidation/reduction process. However, elucidating the mechanism behind the increase in active surface area induced by fluoride is beyond the scope of this article.

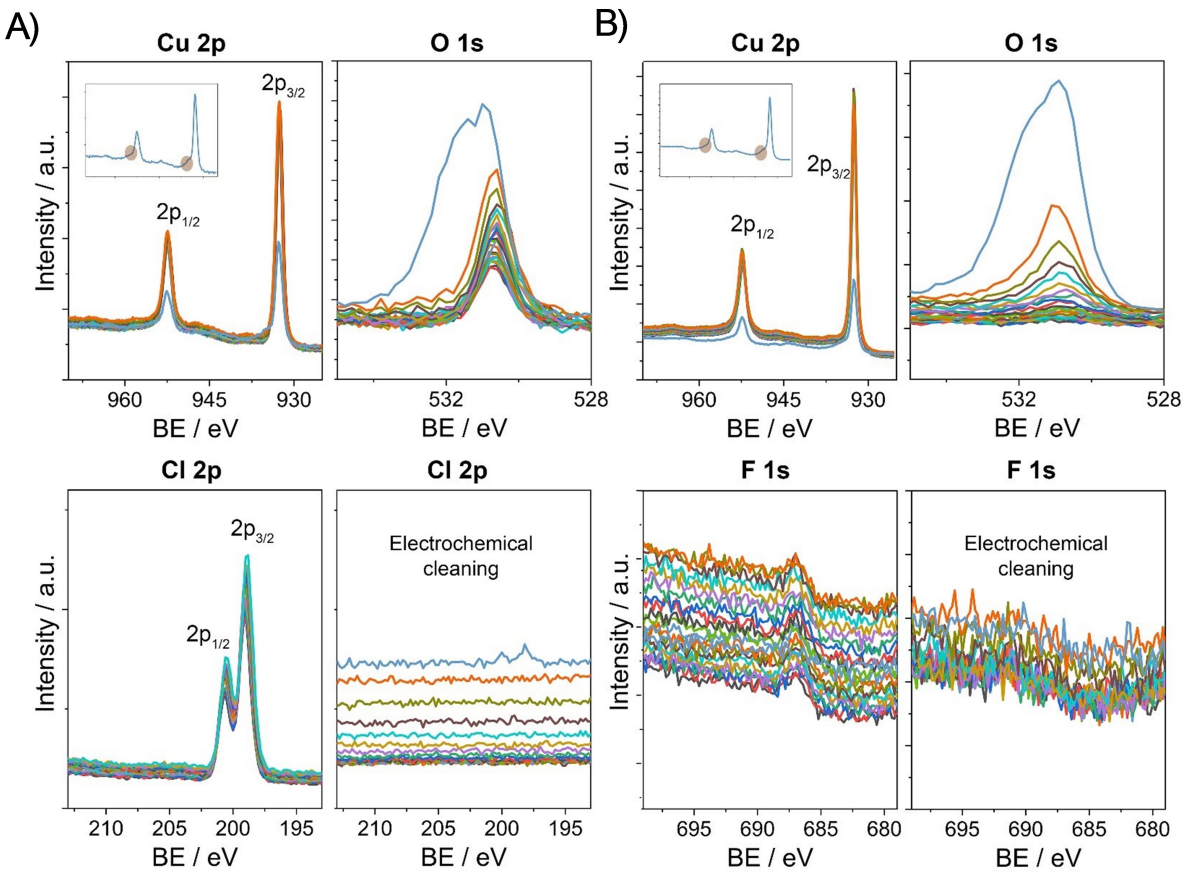

Figure 6. XPS of a Cu(poly) electrode modified in either A) 0.1 M NaCl and B) 0.1 M NaF. We also present the Cl 2p and the F 1s peaks before and after the electrochemical cleaning performed to remove the oxide and halide layer formed after the surface modification treatment in either 0.1 M NaCl or 0.1 M NaF.

Discussion of the Results

To better understand the combined effect of chloride and fluoride on the copper surface modification, we deconvoluted the peaks in the lead UPD cathodic curves from Figure 4B to determine the presence of domains with different geometries. Gaussian mathematical functions from Origin software were used for peak deconvolution.[53] We note that this data-treatment provides a rough estimation of the distribution of geometric domains on copper. The surfaces prepared in this work exhibit complex structures with multiple defect sites and morphology features that cannot be precisely decoupled by only using the lead UPD curves of a few single facets: (111), (100), (110) and (310). Figure 7 shows the peak deconvolution of the lead UPD CVs for three different solutions: A) 0.08 Cl^-:0.02 F^-, B) 0.05 Cl^-:0.05 F^- and C) 0.04 Cl^-:0.06 F^-. We highlighted in orange the peak that is near to the (310) facet in Figure S1. The intensity and area of this peak decrease progressively as the F^-:Cl^- molar ratio increases due to increased surface disorder induced by fluoride. The (n10) peak has an area of 140 $\mu C \cdot cm^{-2}$ in the sample treated with 0.08 Cl^-:0.02 F^- and decreases to 126 $mC \cdot cm^{-2}$ in B) and to 120 $mC\,cm^{-2}$ in C). In terms of the total integrated area in the cathodic curves, the fraction area of the (n10) peak is 0.33 in A), 0.22 in B) and 0.14 in C). Conversely, the voltammetric region between −0.30 V and −0.35 V vs SCE increases considerably in area when we increase the concentration of fluoride in solution. Our voltammetric analysis suggests that fluoride slightly reduces the number of (100) or (n10) sites induced by chloride while causing surface nanostructuring and disorder, with significant formation of defect sites. The exact geometries of the formed nanoclusters cannot be precisely assigned, but we believe that they primarily exhibit (110) or (111) geometry due to the proximity of the lead UPD current features to the (110) and (111) voltammetric zones. A more rigorous analysis of the surface structure should compare the lead UPD CVs of modified copper surfaces with the lead UPD profiles of stepped surfaces in the three zones of the stereographic triangle: [$1\bar{1}0$] with (n-1)(111)x(110) and (n-1)(110)x(111); [$0\bar{1}1$] with n(111)x(100) and n(100)x(111); and [001] with n(100)x(110) and n(110)x(100).. Future studies should aim at analysing the 2(hkl)x(h'k'l') stepped turning points in these three zones. These surfaces contain an equal number of sites with both (hkl) and (h'k'l) geometries, which could help identify specific voltammetric regions for different groups of stepped surfaces.[54]

In this study, we provide new strategies to tune the electroactive surface area and surface geometry of copper using chloride and fluoride halides. Moreover, we provide a direct link between the electrochemical response of copper or lead UPD, and structural information provided with the SEM analysis.[55]

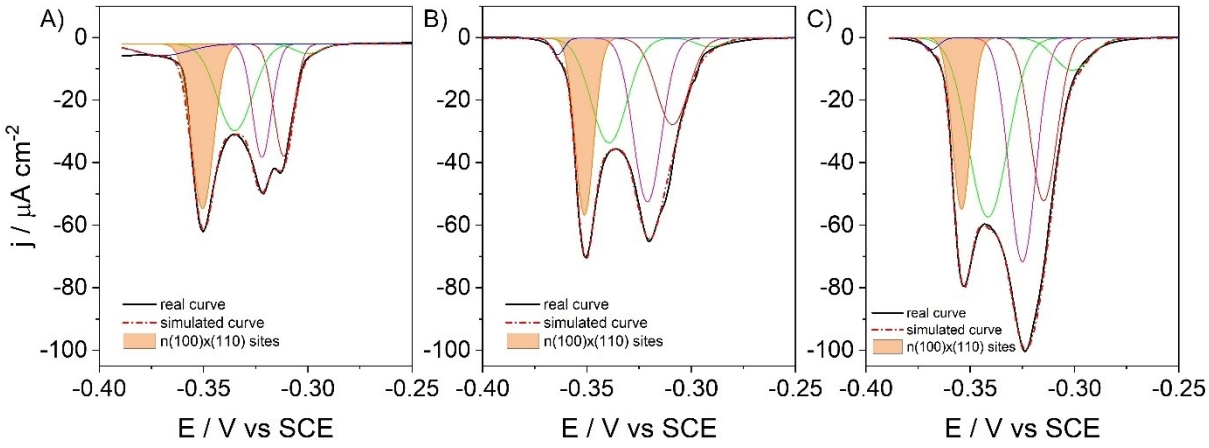

Figure 7. Peak deconvolution of the cathodic voltammetric curves of the lead UPD CVs recorded on the Cu(poly) surfaces modified in: A) 0.02 M NaCl + 0.08 M NaF solution, B) 0.05 M NaCl + 0.05 M NaF solution and C) 0.04 M NaCl + 0.06 M NaF solution. The dashed red line shows simulated curves using gaussian mathematical functions to deconvolute the peaks. The solid black line shows the experimental curve.

Our findings suggestthat lead UPD is sensitive to changes in surface site geometry and provides quantitative insights into surface roughness. The observed increase in surface roughness is attributed to a high population of nanometric features covering the electrodes, as observed in SEM images. Previous studies have emphasized that low-coordinated and defect sites significantly enhance copper catalysis for various reactions, including the hydrogenation of biomass-derived furfural into biofuels[56,57] as well as the conversion of CO_2 toward C2+ products.[10,12,58,59] However, the exact role of defect sites in catalysis or which compounds selectively produce remain unclear. Both ex-situ and in-situ structural characterization techniques provide valuable information about surface structures at the nanometric or atomic scale, albeit limited to small surface areas. Conversely, cyclic voltammetry offers comprehensive structural insights across the entire surface, although it lacks atomic or nanoscale detail. Therefore, integrating cyclic voltammetry with nanoscale or atomic structural characterization methods is essential to elucidate structure-performance relationships in electrochemistry. Furthermore, future studies should incorporate other surface-sensitive spectroscopic techniques, such as grazing incidence X-ray diffraction, to investigate the crystallographic domains of prepared surfaces.[60]

Conclusions

Herein, we investigated the effect of chloride and fluoride on the electrochemical surface modification of copper. We observed that chloride induces the formation of micrometric structures with a (100)x(110) orientation, whereas fluoride only increases surface roughness and forms clusters of nanometric size. We have also established a direct correlation between the electrochemical lead UPD response of copper, and the structural information provided by surface characterization with SEM. Our work provides new insights to rationally prepare and characterize copper surfaces with tailored active site geometries and increased electroactive areas, which is relevant for their use in different applications in electrochemistry.

Notes

The authors declare no competing financial interest.

Associated Content

The supporting information contains complementary CVs of lead UPD on copper single facets and an NaF-treated Cu(poly) sample. FE-SEM and SEM analysis of a Cu(poly) and halide-treated Cu samples; Lead UPD CVs on copper surfaces modified with mixtures of different anions.

Author Contributions

Vicente Pascual Llorens: Investigation, Methodology, Formal analysis, Data curation, Writing – original draft, Visualization.

Albert Serra Ramos: Investigation, Methodology, Formal analysis, Data curation, Writing – original draft, Visualization.

Pedro Mazaira Couce: Methodology, Conceptualization, Writing – review & editing.

María Escudero Escribano: Methodology, Supervision, Writing – review & editing, Resources, Funding acquisition.

Paula Sebastián Pascual: Supervision, Methodology, Formal Analysis, Conceptualization, Writing – original draft, Project administration, Resources, Funding acquisition.

Acknowledgements

We gratefully acknowledge the Villum Foundation for financially supporting this project through a Villum Young Investigator Grant (project number: 53090). MEE, PSP and VPL also knowl-

edge the Danish foundation for financial support through the DFF-Research Project1 (Thematic Research, green transition) grant with number: 0217–00213A. PSP also thanks the Wallenberg Initiative Materials Science for Sustainability (WISE) funded by the Knut and Alice Wallenberg Foundation for funding her current position. We thank Professor Ward van der Stam for valuable discussions in 2022. We acknowledge the Department of Chemistry of the University of Copenhagen and the "Servicios Cientifico Técnicos" of the University of Barcelona for providing facilities to perform this project. We also thank Professor Elvira Gomez from the University of Barcelona for providing valuable discussions for this work.

Conflict of Interests

The authors declare no conflict of interest.

Data Availability Statement

The data that support the findings of this study are available from the corresponding author upon reasonable request.

Keywords: Chloride · Fluoride · Lead underpotential deposition · Active site's geometry · Electroactive surface area

[1] S. Nitopi, E. Bertheussen, S. B. Scott, X. Liu, A. K. Engstfeld, S. Horch, B. Seger, I. E. L. Stephens, K. Chan, C. Hahn, J. K. Nørskov, T. F. Jaramillo, I. Chorkendorff, *Chem. Rev.* **2019**, *119*(12), 7610–7672.
[2] R. Buonsanti, *Nat. Catal.* **2021**, *4*(9), 736–737.
[3] I. E. L. Stephens, K. Chan, A. Bagger, S. W. Boettcher, J. Bonin, E. Boutin, A. Buckley, R. Buonsanti, E. Cave, X. Chang, S. W. Chee, A. H. M. da Silva, P. De Luna, O. Einsle, B. Endrődi, M. E. Escribano, J. V. de Araujo, M. C. Figueiredo, C. Hahn, K. U. Hansen, S. Haussener, S. Hunegnaw, Z. Huo, Y. J. Hwang, C. Janáky, B. S. Jayathilake, F. Jiao, Z. P. Jovanov, P. Karimi, M. T. M. Koper, K. Kuhl, W. H. Lee, Z. Liang, X. Liu, S. Ma, M. Ma, H.-S. Oh, M. Robert, B. R. Cuenya, J. Rossmeisl, C. Roy, M. P. Ryan, E. H. Sargent, P. Sebastián-Pascual, B. Seger, L. Steier, P. Strasser, A. S. Varela, R. E. Vos, X. Wang, B. Xu, H Yadegari, Y. Zhou, *JPhys Energy* **2022**, *4*, 042003.
[4] O. S. Bushuyev, P. De Luna, C. T. Dinh, L. Tao, G. Saur, J. van de Lagemaat, S. O. Kelley, E. H. Sargent, *Joule* **2018**, *2*(5), 825–832.
[5] H. Guzmán, N. Russo, S. Hernández, *Green Chem.* **2021**, *23*(5), 1896–1920.
[6] P. Nilges, U. Schröder, *Energy Environ. Sci.* **2013**, *6*(10), 2925–2931.
[7] Y. Hori, I. Takahashi, O. Koga, N. Hoshi, *J. Mol. Catal. A., Chem* **2003**, *199*(1–2), 39–47.
[8] A. Bagger, W. Ju, A. S. Varela, P. Strasser, J. Rossmeisl, *ACS Catal.* **2019**, *9*(9), 7894–7899.
[9] R. M. Arán-Ais, F. Scholten, S. Kunze, R. Rizo, B. Roldan Cuenya, *Nat. Energy* **2020**, *5*, 317–325.
[10] K. Jiang, Y. Huang, G. Zeng, F. M. Toma, W. A. Goddard, A. T. Bell, *ACS Energy Lett.* **2020**, *5*(4), 1206–1214.
[11] G. H. Simon, C. S. Kley, B. Roldan Cuenya, *Angew. Chem. Int. Ed.* **2021**, *60*(5), 2561–2568.
[12] K.-L. C. Nguyen, J. P. Bruce, A. Yoon, J. J. Navarro, F. Scholten, F. Landwehr, C. Rettenmaier, M. Heyde, B. R. Cuenya, *ACS Energy Lett.* **2024**, *9*(2), 644–652.
[13] C. Choi, S. Kwon, T. Cheng, M. Xu, P. Tieu, C. Lee, J. Cai, H. M. Lee, X. Pan, X. Duan, W. A. Goddard, Y. Huang, *Nat. Catal.* **2020**, *3*(10), 804–812.
[14] W. Ma, S. Xie, T. Liu, Q. Fan, J. Ye, F. Sun, Z. Jiang, Q. Zhang, J. Cheng, Y. Wang, *Nat. Catal.* **2020**, *3*, 478–487.
[15] O. Christensen, S. Zhao, Z. Sun, A. Bagger, J. Vang Lauritsen, S. Uttrup Pedersen, K. Daasbjerg, *J. Rossmeisl. ACS Catal.* **2022**, *12*, 24, 15737–15749.
[16] P. Sebastián-Pascual, M. Escudero-Escribano, *J. Electroanal. Chem.* **2021**, *896*, 115446.
[17] S. A. Nitopi, E. Bertheussen, S. B. Scott, X. Liu, K. Albert, S. Horch, B. Seger, I. E. L. Stephens, K. Chan, J. K. Nørskov, T. F. Jaramillo, I. Chorkendorff, *Chem. Rev.* **2019**, *119*(12), 7610–7672.
[18] J. Solla-Gullón, J. M. Feliu, *Curr. Opin. Electrochem.* **2020**, *22*, 65–71.
[19] L. García-Cruz, V. Montiel, J. Solla-Gullón, *Phys. Sci. Rev.* **2018**, *4*(1), 20170124.
[20] B. Eren, D. Zherebetskyy, L. L. Patera, C. H. Wu, H. Bluhm, G. A. Somorjai, M. Salmeron, *Science (1979)* **2016**, *351*, 475–478.
[21] D. Hochfilzer, A. Tiwari, E. L. Clark, A. S. Bjørnlund, T. Maagaard, S. Horch, B. Seger, I. Chorkendorff, J. Kibsgaard, *Langmuir* **2022**, *38*(4), 1514–1521.
[22] A. Tiwari, T. Maagaard, I. Chorkendorff, S. Horch, *ACS Energy Lett.* **2019**, *4*(7), 1645–1649.
[23] I. Chorkendorff, S. Horch, A. K. Engstfeld, I. E. L. Stephens, T. Maagaard, *Chem. Eur. J.* **2018**, *24*, 17743.
[24] S. J. Raaijman, N. Arulmozhi, A. H. M. da Silva, M. T. M. Koper, *J. Electrochem. Soc.* **2021**, *168*(9), 96510.
[25] V. Climent, J. M. Feliu, *J. Solid State Electrochem.* **2011**, *15*(7–8), 1297–1315.
[26] P. M. Couce, T. K. Madsen, E. Plaza-Mayoral, H. H. Kristoffersen, I. Chorkendorff, K. N. Dalby, W. van der Stam, J. Rossmeisl, M. Escudero-Escribano, P. Sebastián-Pascual, *Chem. Sci.* **2024**, *15*, 1714–1725.
[27] P. Sebastián-Pascual, M. Escudero-Escribano, *ACS Energy Lett.* **2020**, *5*(1), 130–135.
[28] M. Hara, U. Linke, T. Wandlowski, *Electrochim. Acta* **2007**, *52*(18), 5733–5748.
[29] J. Clavilier, *J. Electroanal. Chem.* **1979**, *107*(1), 211–216.
[30] A. Tiwari, H. H. Heenen, A. S. Bjørnlund, T. Maagaard, E. Cho, I. Chorkendorff, H. H. Kristoffersen, K. Chan, S. Horch, *J. Phys. Chem. Lett.* **2020**, 1450–1455.
[31] G. M. Brisard, E. Zenati, H. A. Gasteiger, N. Markovic, P. N. Ross, *Langmuir* **1995**, *11*(6), 2221–2230.
[32] G. M. Brisard, E. Zenati, H. A. Gasteiger, N. M. Marković, P. N. Ross, *Langmuir* **1997**, *13*(8), 2390–2397.
[33] Z. Zhao, J. Zhang, M. Lei, Y. Lum, *Nano Res. Energy* **2023**, *2*, e9120044.
[34] D. Gao, I. Sinev, F. Scholten, R. M. Arán-Ais, N. J. Divins, K. Kvashnina, J. Timoshenko, B. Roldan Cuenya, *Angew. Chem. Int. Ed.* **2019**, *58*(47), 17047–17053.
[35] K. Wandelt, in *Encyclopedia of Interfacial Chemistry* (Eds. K. Wandelt), Elsevier, Oxford, **2018**, pp. 166–181.
[36] A. S. Varela, W. Ju, T. Reier, P. Strasser, *ACS Catal.* **2016**, *6*(4), 2136–2144.
[37] I. Chauhan, H. Bajpai, B. Ray, S. K. Kolekar, S. Datar, K. K. Patra, C. S. Gopinath, *ACS Appl. Mater. Interfaces* **2024**, *16*(20), 26130–26141.
[38] R. Martínez-Hincapié, P. Sebastián-Pascual, V. Climent, J. M. Feliu, *Electrochem. Commun.* **2015**, *58*, 62–64.
[39] P. Sebastián, R. Martínez-Hincapié, V. Climent, J. M. Feliu, *Electrochim. Acta* **2017**, *228*, 667–676.
[40] I. T. McCrum, S. A. Akhade, M. J. Janik, *Electrochim. Acta* **2015**, *173*, 302–309.
[41] H. Kahlert, in *Electroanalytical Methods: Guide to Experiments and Applications* (Eds. F. Scholz, A. M. Bond, R. G. Compton, D. A. Fiedler, G. Inzelt, H. Kahlert, Š. Komorsky-Lovrić, H. Lohse, M. Lovrić, F. Marken, A. Neudeck, U. Retter, F. Scholz, Z. Stojek,), Springer Berlin Heidelberg, Berlin, Heidelberg, **2010**, pp. 291–308.
[42] D.-T. Pham, S.-L. Tsay, K. Gentz, C. Zoerlein, S. Kossmann, J.-S. Tsay, B. Kirchner, K. Wandelt, P. Broekmann, *J. Phys. Chem. C* **2007**, *111*(44), 16428–16436.
[43] H. Matsushima, A. Taranovskyy, C. Haak, Y. Gründer, O. M. Magnussen, *J. Am. Chem. Soc.* **2009**, *131*(30), 10362–10363.
[44] E. Herrero, L. J. Buller, H. D. Abruña, *Chem. Rev.* **2001**, *101*(7), 1897–1930.
[45] E. Plaza-Mayoral, P. Sebastián-Pascual, K. N. Dalby, K. D. Jensen, I. Chorkendorff, H. Falsig, M. Escudero-Escribano, *Electrochim. Acta* **2021**, *398*, 139309.
[46] R. Rizo, B. Roldan Cuenya, *ACS Energy Lett.* **2019**, *4*(6), 1484–1495.
[47] M. C. Biesinger, L. W. M. Lau, A. R. Gerson, R. St. C. Smart, *Appl. Surf. Sci.* **2010**, *257*(3), 887–898.
[48] T. F. Scientific, 2006–2024 Thermo Fisher Scientific Inc., Materials-science, learning-center. 2024 https://www.thermofisher.com/se/en/home/materials-science/learning-center/periodic-table/transition-metal/copper.html.
[49] K. Roy, C. S. Gopinath, *Anal. Chem.* **2014**, *86*(8), 3683–3687.
[50] A. Kundu, M. K. Adak, Y. Kumar, B. Chakraborty, *Inorg. Chem.* **2022**, *61*(12), 4995–5009.

[51] J. Clavilier, R. Faure, G. Guinet, R. Durand, *J. Electroanal. Chem.* **1980**, *107*, 205–209.
[52] D. Strmcnik, M. Escudero-Escribano, K. Kodama, V. R. Stamenkovic, A. Cuesta, N. M. Marković, *Nat. Chem.* **2010**, *2*, 880–885.
[53] E. Garnier, F. J. Vidal-Iglesias, J. M. Feliu, J. Solla-Gullón, *Front. Chem.* **2019**, *7*, 527.
[54] V. Climent, J. M. Feliu, in *Advances in Electrochemical Science and Engineering*, John Wiley & Sons, Ltd, **2017**, pp. 1–57.
[55] L. Jacobse, Y.-F. Huang, M. T. M. Koper, M. J. Rost, *Nat. Mater.* **2018**, *17*(3), 277–282.
[56] J. Li, N. Kornienko, *Chem. Commun.* **2021**, *57*(42), 5127–5130.
[57] S. Liu, Z. Mukadam, S. B. Scott, S. Ch. Sarma, M.-M. Titirici, K. Chan, N. Govindarajan, I. E. L. Stephens, G. Kastlunger, *EES Catal.* **2023**, *1*(4), 539–551.
[58] C. W. Li, J. Ciston, M. W. Kanan, *Nature* **2014**, *508*, 504.
[59] S. B. Scott, T. V. Hogg, A. T. Landers, T. Maagaard, E. Bertheussen, J. C. Lin, R. C. Davis, J. W. Beeman, D. Higgins, W. S. Drisdell, C. Hahn, A. Mehta, B. Seger, T. F. Jaramillo, I. Chorkendorff, *ACS Energy Lett.* **2019**, *4*(3), 803–804.
[60] C. Zhu, Z. Zhang, L. Zhong, C.-S. Hsu, X. Xu, Y. Li, S. Zhao, S. Chen, J. Yu, S. Chen, M. Wu, P. Gao, S. Li, H. M. Chen, K. Liu, L. Zhang, *Chem.* **2020**, *11*, 406–420.

Manuscript received: July 1, 2024
Revised manuscript received: July 23, 2024
Version of record online: September 13, 2024